NMR IN BIOMEDICINE, VOL. 9, 141–155 (1996)

Molar Quantitation of Hepatic Metabolites *In Vivo* in Proton-decoupled, Nuclear Overhauser Effect Enhanced ^{31}P NMR Spectra Localized by Three-dimensional Chemical Shift Imaging

C. W. Li*, W. G. Negendank, J. Murphy-Boesch, K. Padavic-Shaller and T. R. Brown

Department of Nuclear Magnetic Resonance and Medical Spectroscopy, Fox Chase Cancer Center, Philadelphia, PA 19111, USA

Proton decoupling and nuclear Overhauser effect (NOE) enhancement significantly improve the signal-to-noise ratio and enhance resolution of metabolites in *in vivo* ^{31}P MRS. We obtained proton-decoupled, NOE-enhanced, phospholipid-saturated ^{31}P spectra localized to defined regions within the normal liver using three-dimensional chemical shift imaging. Proton-decoupling resulted in the resolution of two major peaks in the phosphomonoester (PME) region, three peaks in the phosphodiester (PDE) region and a diphosphodiester peak. In order to obtain molar quantitation, we measured the NOE of all hepatic phosphorus resonances, and we corrected for saturation effects by measuring hepatic metabolite T_1 using the variable nutation angle method with phase-cycled, B_1-independent rotation, adiabatic pulses. After corrections for saturation effects, NOE enhancement, B_1 variations and point spread effects, the following mean concentrations (mmol/l of liver) (±SD) were obtained: [PME$_1$]=1.2±0.4, [PME$_2$+2,3-DPG]=1.1±0.1, [Pi+2,3-DPG]=2.8±0.5, [GPEth]=2.8±0.7, [GPChol]=3.5±0.6 and [β-NTP]=3.8±0.3. T_1 and NOE enhancement were strongly correlated (r=90), and indicated that the fractional contribution of ^{1}H-^{31}P dipolar relaxation to total ^{31}P relaxation is minimal for NTPs, moderate for PMEs and high for PDEs in liver. Proton-decoupling and NOE enhancement permit one to obtain more information about *in vivo* metabolism of liver than previously available and should enhance the utility of ^{31}P MRS for the study of hepatic disorders.

INTRODUCTION

^{31}P MRS has been used to study a variety of diffuse[1–17] and focal[2,4,7,9,18–24] hepatic diseases. The information available in hepatic ^{31}P MRS has, however, been limited by the inability to resolve individual components of the phosphomonoester (PME) and phosphodiester (PDE) regions of the spectrum. Proton-decoupling of the ^{31}P acquisition provides a means to improve resolution within these regions and has been demonstrated in studies of human liver[25,26] as well as in brain and muscle.[25,27–29] We have recently shown that proton-decoupling, along with nuclear Overhauser effect (NOE) enhancement to improve signal-to-noise ratio (S/N), permits classification of the composition of the PME and PDE regions in *in vivo* ^{31}P spectra of human lymphomas.[30]

Another limitation in extracting information about hepatic metabolites using ^{31}P MRS is the large, broad phospholipid peak centered in the PDE region and extending to underlie the PME, Pi and γ-NTP regions.[31,32] This broad resonance causes uncertainty in spectral fitting and peak intensity analyses because its position, linewidth and lineshape are unknown. Attempts to remove the broad resonance by the use of convolution difference (CD) are not entirely satisfactory because CD affects the intensities of all metabolites (including NTPs), and the choice of CD parameters is somewhat subjective. Moreover, phospholipid resonances are likely to be affected by proton decoupling and NOE enhancement,[33] so their potential variation in different subjects or diseases is another source of concern. Recently, McNamara *et al.*[34] demonstrated effective phospholipid saturation in brain spectra by applying an off-resonance saturation pulse, obviating the need to remove the broad component in post-processing.

A third limitation in studies of hepatic diseases using ^{31}P MRS is the difficulty in quantitating metabolite concentrations. As a result, the intensity of the ^{31}P NMR signal from a metabolite (or group of metabolites in the case of PMEs and PDEs) is typically expressed as a ratio to that of another metabolite. If the two metabolites are changing in the same direction, or if all metabolite concentrations are decreasing in parallel (as might occur in hepatic replacement disorders), then one would miss the opportunity to characterize the disease and/or obtain a diagnostic discriminant by ^{31}P MRS. Molar quantitation of hepatic metabolites *in vivo* has been reported,[3,8,35,36] and has been attempted in three clinical studies.[3,8,15]

To obtain molar concentrations in proton-decoupled ^{31}P spectra requires an accurate definition of the volume of tissue, knowledge of the T_1 of the metabolite signals, a correction for B_1 magnetic field inhomogeneity in the sensitive region of the surface coil, a correction for variations in coil loading and receiver gain, a correction for NOE signal enhancement and a correction for the inter-voxel signal contamination (point-spread effect[37,38]) inherent

* Author to whom correspondence should be addressed.

Abbreviations used: AMP, adenosine monophosphate; BIRP, phase-cycled, B_1-independent rotation, adiabatic pulse; CSI, chemical shift imaging; CV, coefficients of variation; DPDE, diphosphodiester; DPG, diphosphoglycerate; GPChol, glycerophosphocholine; GPEth, glycerophosphoethanolamine; NAD, nicotinamide adenine dinucleotide; NOE, nuclear Overhauser effect; PChol, phosphocholine; PCr, phosphocreatine; PDE, phosphodiester; PEP, phosphoenolpyruvate; PEth, phosphoethanolamine; Pi, inorganic phosphate; PME, phosphomonoester; S/N, signal-to-noise ratio; SAR, specific absorption rate; TPP, triphenyl phosphate.

CCC 0952–3480/96/040141–15

Received 12 October 1995
Accepted (revised) 26 March 1996

in phase-encoding used to localize spectra with chemical shift imaging (CSI).[39] We report the development of procedures to obtain molar quantitation of hepatic metabolites in proton-decoupled, NOE-enhanced, phospholipid-saturated ^{31}P MR spectra obtained with surface probes and localized in three dimensions using MRI-directed CSI.

EXPERIMENTAL

Instrumentation and ^{31}P MRS

Twelve healthy adults (five males, seven females, aged 25–60) participated in these studies. No attempt was made to modify or control the diet of the volunteers before MR spectroscopy was performed and they were not fasting; however, subjects were studied at 4–8 h post-prandial to avoid meal-induced effects on the ^{31}P metabolites.[40] Studies were done in a Helicon 1.5 T clinical imager/spectrometer (Siemens AG, Erlangen, Germany). The subject was positioned supine and a dual-tuned surface coil placed laterally over the liver. The coil assembly consisted of a circular 15 cm diameter ^{31}P coil and a larger 18×22 cm ^{31}P coil as shown in Fig. 1. The ^{1}H coil was in a figure-8 or butterfly configuration, and was curved on a 30 cm radius to permit apposition to the subject's right side. The proton element was used for MR imaging, shimming and proton-decoupling. MR images of 10 mm thickness were obtained in nine slices in each of three dimensions using a gradient echo method with TR=310 ms and TE=15 ms. Shimming was initially performed by manual adjustment of lower- and higher-order shim currents and more recently by automatic adjustment of these currents using an autoshimming algorithm based on three-dimensional ^{1}H CSI.[41,42] The linewidth at half height of the water resonance of the nonlocalized ^{1}H spectrum was typically 20–40 Hz. Nonlocalized ^{31}P spectra were collected with and without ^{1}H-decoupling to ensure proper functioning of the decoupler. They were obtained with 250 μs rectangular pulses, TR=1 s and 64 acquisitions. Three-dimensional CSI datasets were acquired with an 8×8×8 matrix, a voxel size of 3×3×3 (27 cm^3) or 4×4×4 (64 cm^3), a 250 μs rectangular pulse, 512 time points, a sweep width ±1 kHz and a TR=1 s. One to four acquisitions were obtained for each phase encoding step for a total acquisition time of 8.5–34 min depending on the study. A 45° nutation angle in the center of the region of interest at a depth of about 5–9 cm into the antero-lateral right lobe of the liver was set by use of a reference signal from triphenyl phosphate (TPP) located in the plane of the coil and the B_1 field plot.

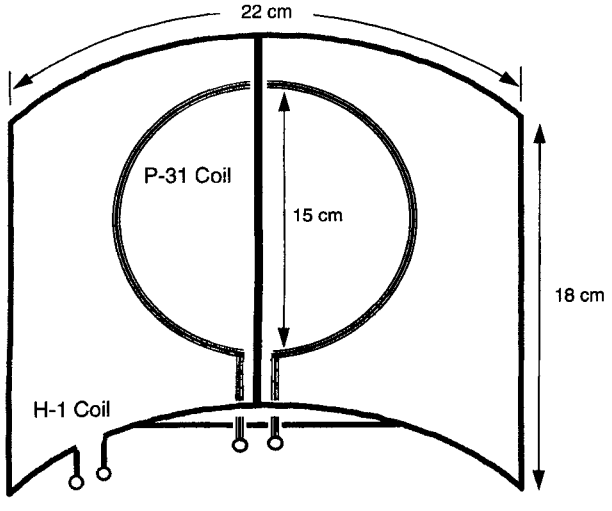

Figure 1. A schematic view of the ^{1}H ^{31}P dual tuned coil. The ^{1}H coil was curved on a 30 cm radius to permit apposition to the subject's right side.

Removal of the broad phospholipid PDE peak was accomplished with a 204.8 ms gaussian saturation pulse (12 Hz bandwidth) 290 Hz downfield from phosphocreatine (PCr).[34] The off-resonance location and power (4.5 W to the coil) of the saturation pulse were chosen to remove the maximum amount of phospholipid peak area with minimal effect on the overlying PME, Pi and PDE peaks. With this procedure, we estimate that <8% of the intensities of the PME, Pi and PDE peaks was lost.

Proton-decoupling

Broadband decoupling was implemented using WALTZ-4 modulation gated with a sequence-programmable signal from the spectrometer. The decoupler channel was constructed as described elsewhere.[29] Bi-level decoupling was used with a power level of 16 W during acquisition (256 ms) situated 1 ppm below the water resonance, dropping to 2 W between acquisitions for maintenance of NOE. The average specific absorption rate (SAR) was calculated taking into account the power attenuation by the transmission line; the duty cycle; and the fraction of the power delivered to the tissue, which is proportional to $(1\text{-}Q_{loaded}/Q_{unloaded})$. The average power delivered to the tissue was 2.9 W (for TR=1 s). In the case of the 18×22 cm rectangular ^{1}H surface coil with a sensitive volume of about 2.2 l, this gives an SAR of approximately 1.3 W/kg.

BIRP Pulse

To permit measurement of T_1 in the presence of B_1 field inhomogeneities of the surface coil, we obtained uniform, arbitrary nutation angles by using the phase alternation modification of the B_1-independent rotation (BIR-4) pulse,[43] referred to as the 'BIRP' pulse.[44] The original BIR-4 pulse wave forms were generated using a FORTRAN program provided by Dr Michael Garwood at the University of Minnesota, Minneapolis. The BIRP pulse was implemented with 512 points of amplitude and phase values with a duration of 6.1 ms. The peak power to the coil was 450 W. Taking into account the power attenuation by the transmission line, the duty cycle and the fraction of the power delivered to the tissue, the average power delivered to the tissue was 2.3 W when using a TR of 1.0 s. In the case of the 15 cm circular surface coil with a sensitive volume of about 1.3 l, this gave an SAR of approximately 1.7 W/kg. The sensitive volume was approximated by the volume which contained all regions with sensitivity 0.3 relative to a point in the center of the coil. In the case of the 15 cm circular coil, this volume was approximated by a hemisphere with a radius of 8.5 cm.

T_1 Measurement

The T_1s of hepatic metabolites were measured in four healthy volunteers by using the variable nutation angle method[45,46] with the BIRP pulses. By systematically varying

the nutation angle, a plot of $I(\theta)/\sin(\theta)$ vs $I(\theta)/\tan(\theta)$ for a single T_1 will provide a straight line with the slope of $e^{-TR/T1}$, where I is the signal intensity and θ is the applied nutation angle. T_1 is obtained by a linear regression analysis of the data. CSI-localized liver spectra were obtained with nutation angles of 20, 40, 60 and 80°. Three-dimensional CSI datasets were acquired with an $8\times8\times8$ matrix of 64 ml voxels, first using a TR of 1.0 s with two averages per phase-encoding step in order to obtain the optimal range of TR/T_1 for metabolites with long T_1, such as PDEs, and then using a TR of 0.5 s with five averages per phase-encoding step in order to obtain the optimal range of TR/T_1 for metabolites with short T_1, such as NTPs. Fifteen pre-scans were applied before each measurement to establish a steady-state magnetization. The transmitter frequency was set between γ-NTP and α-NTP resonances. The SAR in this measurement, in which proton-decoupling, NOE enhancement, phospholipid saturation and the BIRP pulse were all implemented, was 5.5 W/kg when using a TR of 0.5 s.

NOE enhancement

NOE enhancements were measured to correct for intensity increases in the absolute concentration calculation. Localized spectra were acquired with two-dimensional CSI localization in the axial plane (the third dimension is defined by the sensitive volume of the surface coil). A BIRP pulse with a 90° nutation angle was followed by two phase encoding gradients. The 8×8 phase encoding steps resulted in a spatial resolution in the region of interest in the liver of about $5\times5\times8$ cm. A total of 512 time points, a SW=±1 kHz, a TR=20 s and one acquisition for each phase encoding step resulted in a total acquisition time of 22 min. Two measurements were performed sequentially with and without the continuous component of the bi-level decoupling applied. NOE enhancements (η) were calculated as the differences in the peak areas of these spectra divided by the peak areas of those with no enhancement.

Data analysis

Data were processed with software and techniques developed in our laboratory.[29,47] The MR images were overlaid with 8×8 grids indicating the ^{31}P voxel positions. Three-dimensional CSI data sets were Fourier transformed in the three spatial dimensions. The phase-correction parameters for the spectrum obtained from the nonlocalized FID were used to phase-correct all spectra in the CSI array. Based on the corresponding images, three-dimensional CSI data sets were voxel shifted to center one or more voxels on liver. The CSI data from one or more voxels within regions of interest were extracted and processed using NMR1 software (New Methods Research, Syracuse, NY). A 3 Hz Lorentzian filter was applied before the final Fourier transformation in the time dimension. The baseline was straightened using the NMR1 semi-automatic baseline deconvolution software. Peak integrals were estimated by fitting to Lorentzian lineshapes. Since the glycerophosphocholine(GPChol) signal was consistently well resolved in the proton-decoupled ^{31}P spectrum and is known not to change its chemical shift over the physiological pH range, chemical shifts of Pi were measured relative to GPChol, which was set to 0.49 ppm (phosphoric acid=0.0 ppm), and were converted to pH using the Henderson–Hesselbach relation[48] with the parameters $pK_a=6.718$, $\delta_{acid}=0.591$ and $\delta_{alkaline}=3.187$.

Metabolite Quantitation

Quantitation was performed using the B_1 field plot of the coil and a single reference signal from a standard placed in the plane of the coil. Corrections were made for B_1 field inhomogeneity, variable coil loading, NOE enhancement, saturation factors and contamination associated with the point spread function (PSF).

A detailed analysis of point spread function effects in quantitation of metabolites in three-dimensional CSI spectra has been previously reported.[49] In a phase-encoding technique such as CSI, the discrete Fourier transform of a finite sampling dataset produces a sinc-shaped ringing artifact or point spread function in the reconstructed spatial distribution of the signal intensity.[37,38] The PSF conveys the signal contribution from every region in the sample to a voxel. As a result, the reconstructed localized signal at position $\mathbf{r}$, $S_{rec}(\mathbf{r})$, contains different degrees of contamination from the other voxels in the CSI dataset. The relation between $S_{rec}(\mathbf{r})$ and the PSF is expressed by the equation

$$S_{rec}(\mathbf{r})=\int_{\text{Sample}} s(\mathbf{s})\cdot PSF(\mathbf{r}-\mathbf{s})\cdot d^3\mathbf{s}, \quad (1)$$

where $s(\mathbf{s})$ is the original local signal density at position $\mathbf{s}$ (signal intensity per unit volume of sample) and $\mathbf{s}$ is a running variable over the sample.

The original local signal density at position $\mathbf{r}$, $s(\mathbf{r})$ can be related to the sample concentration, $C(r)$, by the following equation

$$\mathbf{s}(\mathbf{r})=K\cdot C(\mathbf{r})\cdot(1+\eta)\cdot K_{sat}(\mathbf{r})\cdot B_{1xy}(\mathbf{r}). \quad (2)$$

K is a contant which relates to the whole system gain, η is the NOE enhancement factor, $K_{sat}(\mathbf{r})$ is the saturation factor which is given by

$$K_{sat}(\mathbf{r})=(1-e^{-TR/T_1})\cdot\sin\phi(\mathbf{r})/[1-\cos\phi(\mathbf{r})\cdot e^{-TR/T_1}] \quad (3)$$

where $\phi(\mathbf{r})$ is the nutation angle at the position $\mathbf{r}$ and T_1 is the measured hepatic metabolite T_1 value. $B_{1xy}(\mathbf{r})$ is the B_1 field distribution of the surface coil and was obtained from simultations using the Biot–Savart law.[50] Since the delay time is short in the three-dimensional CSI sequence (800 μs), we neglect the signal loss due to the T_2 relaxation. By combining eqs (1) and (2), the reconstructed localized signal intensity can be expressed as

$$S_{rec}(\mathbf{r})=K\int_{\text{Sample}} C(\mathbf{r})\cdot(1+\eta)\cdot K_{sat}(\mathbf{s})\cdot B_{1xy}(\mathbf{s})\cdot PSF(\mathbf{r}-\mathbf{s})\cdot d^3\mathbf{s} \quad (4)$$

Since $S_{rec}(\mathbf{r})$ can be obtained by Fourier transformation of the CSI dataset, the concentration of the sample can be reconstructed from eq. (4).

In practice, several assumptions can be made to simplify the solution of eq (4): (a) the concentration is uniform over the sample; (b) the T_1 of the metabolites are constant over the sample; (c) the ηs of the metabolites are constant over

the sample; and (d) the sample can be represented by a simple geometrical shape, which in this study is a sphere. The assumptions in (a) and (b) are reasonable because the position of the voxel is superficial enough to avoid large blood vessels and the ^{1}H images show relatively homogeneous tissue. The assumption in (c) is reasonable because the larger size of the ^{a} coil than of the ^{31}P coil and the selection of the power levels permit degrees of ^{1}H uniform ^{1}H-decoupling and NOE enhancement within the region of interest. The point spread effect correction in the calibration procedure is based on the assumption that the region of the liver within the sensitive volume of the coil can be approximated by a sphere. The point spread effect correction is influenced by the geometry of the region of interest, and the extent of this influence is still under investigation.[49] For this special case of a voxel containing liver surrounded by a considerable amount of liver, the geometry is not critical. Since PCr is absent or negligible in the localized hepatic spectra (Figs 3 and 4), we assume the other signals from muscle are also negligible. The size and the imaginary center of the sphere vary among subjects and are measured from the MR images. Figure 2 shows an example of the selection of sphere size and position for the PSF correction in one of the liver quantitation studies. The radius of the sphere varied among the volunteers from 6.5 to 10.0 cm. Since the sensitivity drops with the distance from the surface coil, the point spread effect in the selected voxel is mainly contributed by signals in the hemisphere which is closest to the coil.

With these assumptions, the sample concentration (C_0) and η become constants which drop out of the integral of eq. (4). The sample (i.e. the liver) is approximated by a

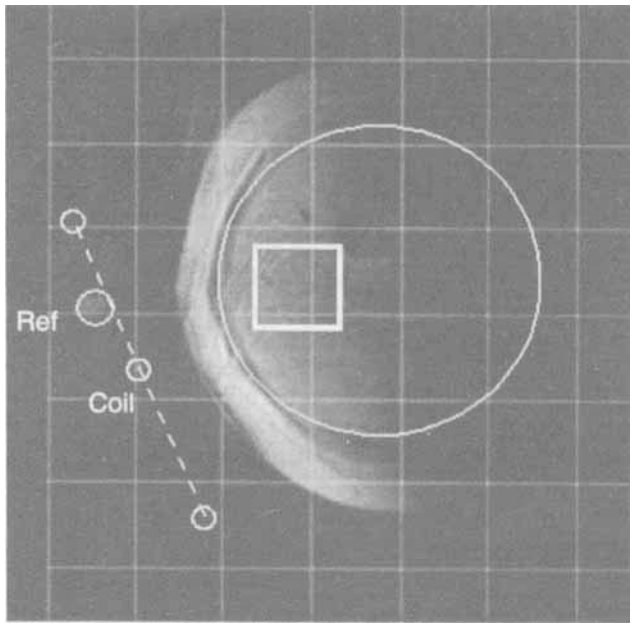

Figure 2. Example of the selection of the sphere size and position for the PSF correction. The position of the 15 cm ^{31}P surface coil, the triphenyl phosphate-containing reference and the representative localized voxel are shown. The size and position of the sphere are chosen to fit the contour of the portion of the liver which is closest to the coil.

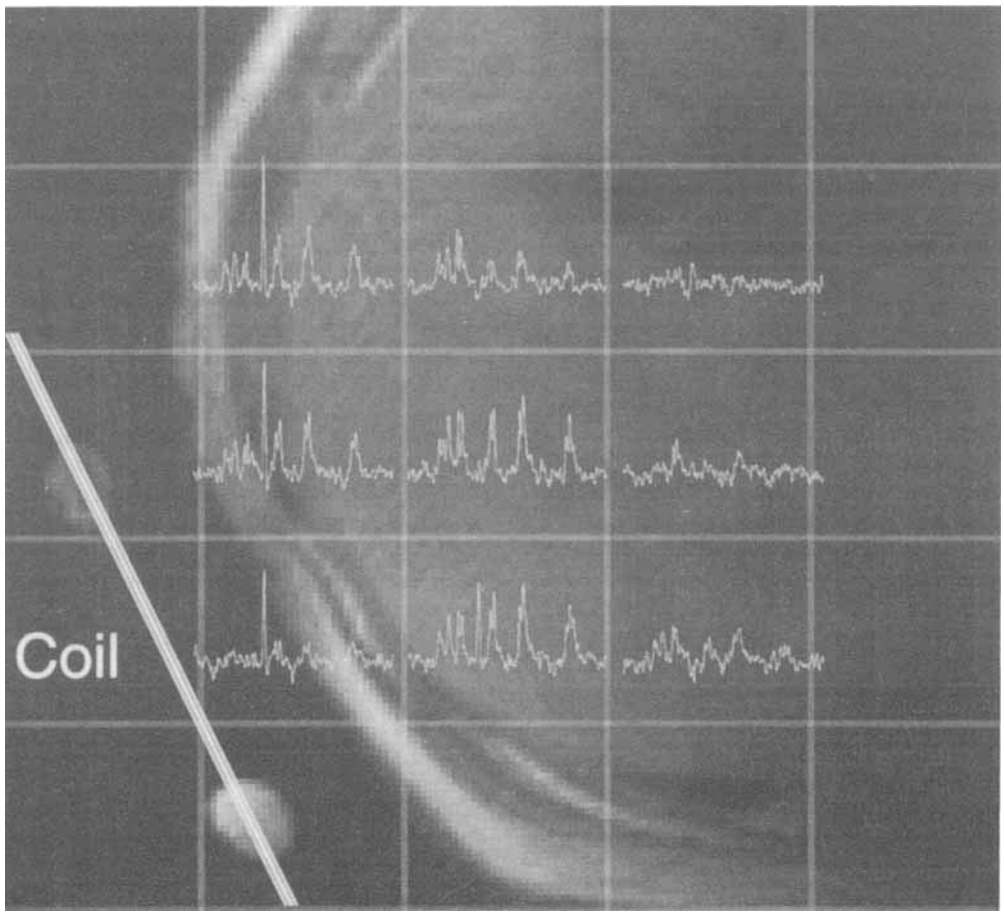

Figure 3. Example of the proton-decoupled three-dimensional CSI ^{31}P MRS study in a volunteer. An axial image has the grid overlaid on it to show the positions of 25 of the MRS voxels in this slice and spectra from nine of these voxels. The position of the 15 cm ^{31}P surface coil is also illustrated in this image.

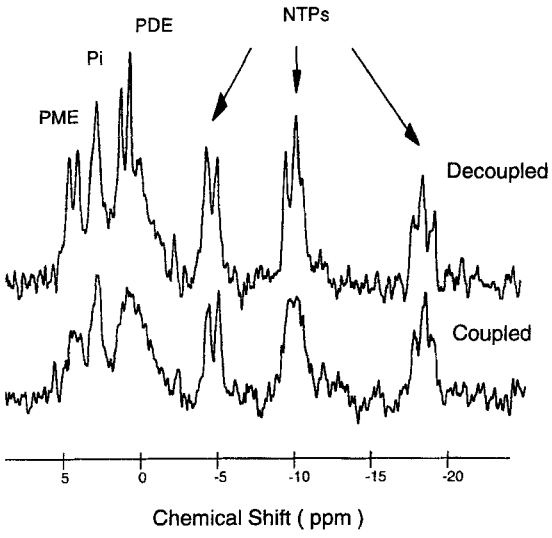

Figure 4. Three-dimensional CSI-localized ^{31}P spectra with and without proton-decoupling and NOE enhancement. Each spectrum is from a 54 ml voxel and required 34 min of data collection.

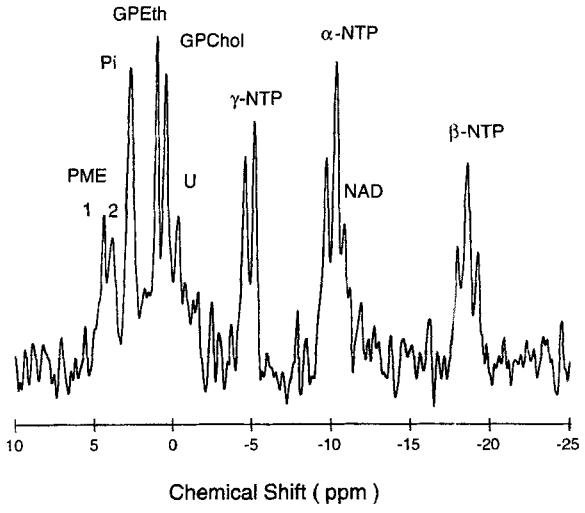

Figure 5. Three-dimensional ^{31}P spectrum with metabolite peak assignments.

sphere, and the reconstructed localized signal for a voxel centered at position **r** becomes

$$S_{rec}(\mathbf{r}) = K \cdot C_0 \cdot (1+\eta) \cdot \int_{\text{Sphere}} K_{\text{sat}}(\mathbf{s}) \cdot B_{1xy}(\mathbf{s}) \cdot PSF(\mathbf{r}-\mathbf{s}) \cdot d^3\mathbf{s}$$
$$= K \cdot C_0 \cdot F, \quad (5)$$

where $F = (1+\eta) \cdot \int_{\text{Sphere}} K_{sat}(\mathbf{s}) \cdot B_{1xy}(\mathbf{s}) \cdot PSF(\mathbf{r}-\mathbf{s}) \cdot d^3\mathbf{s}$. The sample concentration can be expressed as

$$C_0 = \frac{S_{rec}(\mathbf{r})}{K \cdot F}. \quad (6)$$

To determine the value of K, a reference of known concentration was used to correlate the detected signal intensity with the number of spins. A small reference sphere (2 cm^3) filled with 1.9 M TPP solution was placed in the plane of the surface coil, but 3 cm from the coil center to prevent interference caused by the central conductor of the proton coil. A fully relaxed nonlocalized spectrum was collected from the TPP reference with a 90° nutation angle. This signal intensity is

$$S_{ref} = K \cdot C_{ref} \cdot V_{ref} \cdot B_{1xy,\,ref}. \quad (7)$$

Here, V_{ref} is the volume of the reference, C_{ref} is the concentration of the TPP reference (mM) and $B_{1,\text{ref}}$ is the B_1 field in the TPP reference.

The concentration of hepatic metabolites, C_0, is calculated by combining eqs (6) and (7):

$$C_0 = C_{ref} \cdot \frac{S_{rec}/F}{S_{ref}/(B_{1xy,\,ref} \cdot V_{ref})}. \quad (8)$$

Since it is not feasible to obtain all of the data required to perform a rigorous quantitation study in one subject at one time, we used mean values of T_1s and NOE enhancements that were obtained in separate series of experiments.

RESULTS

The procedure by which we obtain MRI-directed ^{31}P MRS localized in liver using three-dimensional CSI is illustrated in Fig. 3. Figure 3 is an axial image with overlying grids which show the positions of 25 of the MRS voxels in this slice and the spectra from the nine central voxels. The position of the 15 cm ^{31}P surface coil is also illustrated in this image. The spectra from voxels at the surface of the body contain PCr from muscle in the chest wall. Voxels localized entirely within the liver contain no PCr. Spectra from voxels centered 10 cm or more from the coil are noisy because they are beyond the sensitive volume of the coil. The central voxel is taken to best represent hepatic metabolism. The effect of proton decoupling and NOE-enhancement on the ^{31}P MR spectrum is shown in Fig. 4. Decoupling permits excellent resolution of the separate major components in the PME and PDE regions, and decoupling plus NOE enhancement increase the S/N of most of the resonances in the spectrum.

The assignment of metabolites to peaks in the localized proton-decoupled ^{31}P spectrum of liver is shown in Fig. 5. Table 1 lists the chemical shifts of the major peaks observed in 10 subjects. The dominance of glycerophosphoethanolamine (GPEth) and GPChol in the PDE region and relative intensities of the GPEth and GPChol peaks are very similar to observations *in vitro* in fresh human liver biopsies.[51] The

Table 1. Chemical shift (in ppm) of ^{31}P metabolites in normal liver (mean ± SD, n = 10)

Metabolite	Chemical Shift (ppm)
PME_1	4.36 ± 0.05
PME_2	3.84 ± 0.02
Pi	2.69 ± 0.05
GPEth	1.05 ± 0.01
GPChol	0.49
Unknown	−0.30 ± 0.10
γ-NTP	−4.88 ± 0.04
α-NTP	−10.00 ± 0.03
DPDE(NAD)	−10.78 ± 0.04 (n=5)
β-NTP	−18.58 ± 0.04

composition of the two well-resolved peaks in the PME region is, however, not easy to determine. In perchloric acid extracts studied at pH 8.9, the most prominent peak in the PME region was adenosine monophosphate (AMP).[51] At the pH observed in liver *in vivo* (7.24), the AMP peak should occur at around 4.2 ppm, while the PME_1 peak we observe is centered at 4.36 ppm. Consequently it is possible that other metabolites, such as sugar phosphates, contribute to this peak. In extracts[51] there were significant contributions to PME from coenzyme A and the 2P- and 3P-peaks of 2,3-diphosphoglycerate (DPG), the latter presumably in erythrocytes. At the pH of blood, erthyrocyte 2,3-DPG peaks are at 3.8 and 2.8 ppm.[52] Since the vascular volume of the human liver is approximately 25%,[53] it is likely that signals from 2,3-DPG contribute to PME_2 and to Pi. In fact, the Pi peak in proton-decoupled spectra is usually noted to have a hump on its downfield side at 2.8 ppm or to be a doublet (e.g. Figs 4,6,7,12). However, it is unlikely that 2,3-DPG signals account for all of the PME_2 or Pi peaks. As will be shown below, PME_2 has a concentration of 1.1 mmol/l of liver and Pi 2.8 mmol/l of liver. With a vascular volume of 25% and an erythrocyte [2,3-DPG] of 4.2 mmol/l cells, the hepatic [2,3-DPG] would be 0.5 mmol/l of liver which would account for 45% of the PME_2 signal and 18% of the Pi signal.

The Pi chemical shift of 2.69 ± 0.05 ppm corresponds to an apparent pH of 7.34 ± 0.06, in agreement with previously reported studies.[7,25,35] However, it is likely that both 3P-DPG and Pi contribute to this peak. From 10 studies on six subjects which show obvious split peaks in the Pi, the chemical shifts are 2.89 ± 0.09 and 2.59 ± 0.06. Since 2.89 is close to the position of 3P-DPG in erythrocytes, it is likely that the Pi chemical shift is 2.59 and that hepatic pH is closer to 7.24 than to 7.34.

The unknown PDE peak at -0.30 ppm, which was also observed in decoupled spectra by Wicklow *et al.*[26] is at the proper position for phosphoenolpyruvate (PEP), which has been documented in rat liver[54] and has been observed in the liver of rats infused with L-alanine.[55] Three major peaks at -4.88, -10.00 and -18.58 ppm are due to the three phosphates of nucleoside triphosphates (NTP). Diphosphodiesters (DPDE), which in liver are predominantly nicotinamide adenine dinucleotide (NAD) and NADH,[51] are visible as a shoulder on the upfield side of the α-NDP peak at -10.78 ppm.

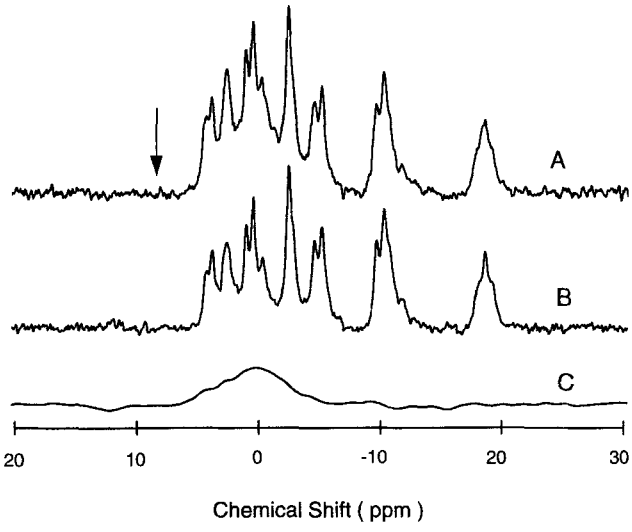

Figure 6. Non-localized ^{31}P spectra from the liver (a) without and (b) with phospholipid saturation. The difference between these two spectra is shown in (c). The arrow indicates the position of the off-resonance selective gaussian pulse. Each spectrum was collected with a 250 μs rectangular pulse, 64 acquisitions and TR = 1 s.

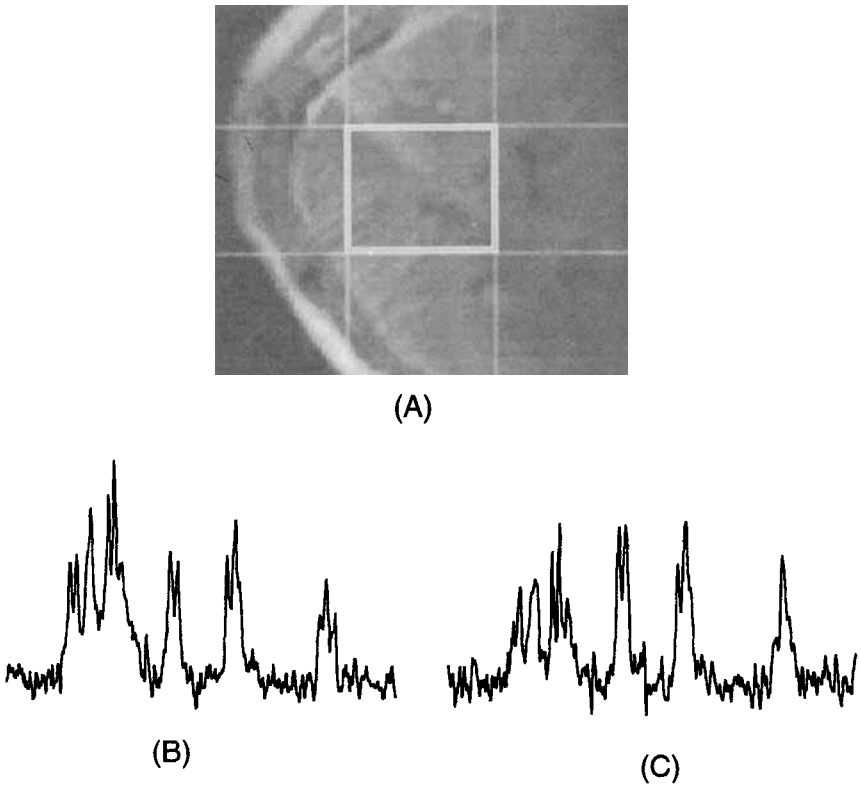

Figure 7. Three-dimensional localized ^{31}P MRS with and without phospholipid saturation. (a) Axial image with the grid overlaid on it. The spectra corresponding to the highlighted region are shown without (b) and with (c) phospholipid saturation.

Phospholipid resonance saturation and temporal reproducibility

The broad resonance underlying the PME-through-PDE region in liver appears to be primarily from phospholipids in the endoplasmic reticulum.[33] Removal of this resonance by saturation is shown in Fig. 6. In 10 separate nonlocalized spectra obtained from five subjects, the broad phospholipid resonance [Fig. 6(c)] had a linewidth of 4.8±0.5(SD) ppm and a peak position of 0.1±0.2 ppm. The use of phospholipid saturation in proton-decoupled, three-dimensional CSI-localized ^{31}P MRS is shown in Fig. 7.

To evaluate the reproducibility of the phospholipid saturation technique, one subject was studied five times without saturation and seven times with saturation over a period of 2 months. Since molar quantitation was not obtained in all cases, the results are expressed as metabolite signal intensity fractions. Mean metabolite fractions and their coefficients of variation (CV) from spectra localized to the liver are shown without and with saturation in columns (2) and (3) in Table 2. Phospholipid saturation did not introduce greater variations in the data; in fact it resulted in smaller variations for several of the peak intensity fractions.

Intraindividual variations were examined in serial ^{31}P MR spectra. In short-term studies neither the subject nor the coil were removed, in order to determine variations resulting primarily from statistical noise. In long-term studies, the same subject returned seven times over a period of 2 months, in order to determine additional variance resulting from coil placement, subject cooperation, instrument drift and possibly diet. The results of long- and short-term reproducibility in phospholipid-saturated spectra are compared in columns (3) and (4) in Table 2. The CVs for the six major metabolite signals (total PME, total PDE, Pi and NTPs) vary from 6 to 17% (average 11%) in the long-term study and from 4 to 11% (average 8%) in the short-term study. For the separate components of the PME and PDE regions, the CVs are larger (17–35%). To some extent these reflect variations in resolution and consequent uncertainties in peak integration. It is possible that physiological variations (eg, diet[40]) contribute as well. If we assume that the short-term study provides primarily an index of noise inherent in the system and the measurement, then only slightly greater variability was introduced when a subject was studied at various times over several weeks.

Table 2. Intra-individual temporal reproducibility of proton-decoupled, three-dimensional CSI-localized ^{31}P MRS and the effects of phospholipid saturation. Metabolite signal intensities are expressed as fractions of total phosphorus signal intensity. Means and CV(%) are shown

(1) Metabolite	(2) Long-term (n=5) without saturation	(3) Long-term (n=7) with saturation	(4) Short-term (n=5) with saturation
PME_1	0.05(30%)	0.04(20%)	0.04(24%)
PME_2	0.05(48%)	0.04(24%)	0.04(22%)
PME[a]	0.10(15%)	0.08(17%)	0.07(11%)
Pi	0.12(22%)	0.12(8%)	0.13(13%)
GPEth	0.06(57%)	0.08(34%)	0.08(17%)
GPChol	0.04(46%)	0.06(28%)	0.06(26%)
Unknown	0.24(22%)[c]	0.06(35%)	0.06(24%)
PDE[b]	0.34(4%)[c]	0.20(8%)	0.21(4%)
γ-NTP	0.12(19%)	0.16(12%)	0.16(6%)
α-NTP+NAD	0.19(11%)	0.26(9%)	0.25(6%)
β-NTP	0.11(17%)	0.17(12%)	0.17(8%)

[a]PME is the summation of PME_1 and PME_2.
[b]PDE is the summation of GPEth, GPChol and unknown.
[c]Includes the phospholipid broad resonance.

Performance of the BIRP pulse

Before applying the BIRP pluse to measure ^{31}P T_1 relaxation times and NOE enhancements in human liver, we tested its performance in the spatial and frequency-offset distributions using a $20\times10\times4$ cm^3 rectangular phantom containing phenylphosphate, inorganic phosphate and tripolyphosphate. Figure 8(a) shows an axial image with overlying grids which indicate the positions of the MRS voxels ($2.5\times2.5\times2.5$ cm^3) in this slice. A nonlocalized spectrum with a 45° BIRP pulse is shown in Fig. 8(b). The frequency range of the signals, ±500 Hz, is wider than that of the ^{31}P signals in liver. Figure 8(c) and (d) show the spectra from the highlighted voxels obtained with 45 and 180° nutation angle BIRP pulses, respectively. The null signal following a 180° nutation angle occurs uniformly to a depth that is 3/4 of the coil diameter, and occurs throughhout the frequency range of the spectra.

The accuracy of the nutation angles set by the BIRP pulse was tested by using a 5 ml spherical phantom which contained phenylphosphate and inorganic phosphate with nominal nutation angles in the range of 10–90° at increments of 10° and TR>$5T_1$. The sample was positioned 5 cm away from the ^{31}P surface coil. The carrier frequency was positioned between the two resonances shown in Fig. 9(a). Figure 9(b) shows the fully relaxed signal intensity of these resonances as a function of the nutation angle ϕ. The BIRP pulse generated the correct sinusoidal dependence of signal intensity within an error of only a few per cent (the difference between the nominal nutation angle and the apparent nutation angle ranged from −1 to 4° for phenylphosphate and −4 to 1° for inorganic phosphate). The apparent nutation angle was determined from the arcsine of the ratio of the signal at the nominal nutation angle to the signal measured with ϕ=90°.

To test the use of the variable nutation angle method to measure the T_1 in ^{31}P spectra obtained with surface coils, nonlocalized T_1 measurements were performed on four 5 ml samples of phenylphosphate and inorganic phosphate doped with different amounts of $NiCl_2$ to give a range of T_1 values from 0.5 to 7.5 s. The T_1 measurements were done first by a standard inversion-recovery method and then by the variable nutation angle method. Invasion-recovery experiments were performed with TR>$5T_1$. In the variable nutation angle experiment, four nutation angles were used (20, 40, 60 and 80°) and the TR values were chosen to fall in the range $0.1<TR/T_1<2.0$. Fifteen pre-scans were applied before each measurement to establish a steady-state magnetization. The results, shown in Fig. 10, demonstrate that T_1 measurements by the variable nutation angle method and the inversion-recovery method agree within 15%.

T_1 of hepatic metabolite signals

Figure 11 illustrates the measurement of the T_1 of proton-decoupled, three-dimensional CSI-localized ^{31}P signals of hepatic metabolites. It includes a peak (GPEth+GPChol +unknown) with long T_1 [measured with TR=1.0 s, Fig. 11(a)], and one (α-NTP+NAD) with a short T_1 [measured

with TR = 0.5 s, Fig. 11(c)]. The corresponding plots of $I(\phi)/\sin(\phi)$ against $I(\phi)/\tan(\phi)$ in Fig. 11(b) and (d) show a linear correlation of 0.98 in GPEth+GPChol and 0.99 in α-NTP+NAD and give T_1s of 4.6 and 0.5 s, respectively. The T_1 of PCr from a voxel which included mostly chest wall muscle was calculated in each subject and compared to previous studies in muscle to help verify the T_1 measurements *in vivo*. The results of hepatic metabolite T_1 measurements are summarized in Table 3.

NOE Enhancements

The position of the coil, the CSI grids in the axial plane and the ^{31}P voxels of interest for this experiment are shown in Fig. 12(a). The localized ^{31}P spectra without the constant component of bi-level decoupling from the two voxels are shown in Fig. 12(b) and (d). The voxel from which the spectrum is shown in Fig. 12(d) was included because it contains muscle, the PCr signal of which has a known NOE

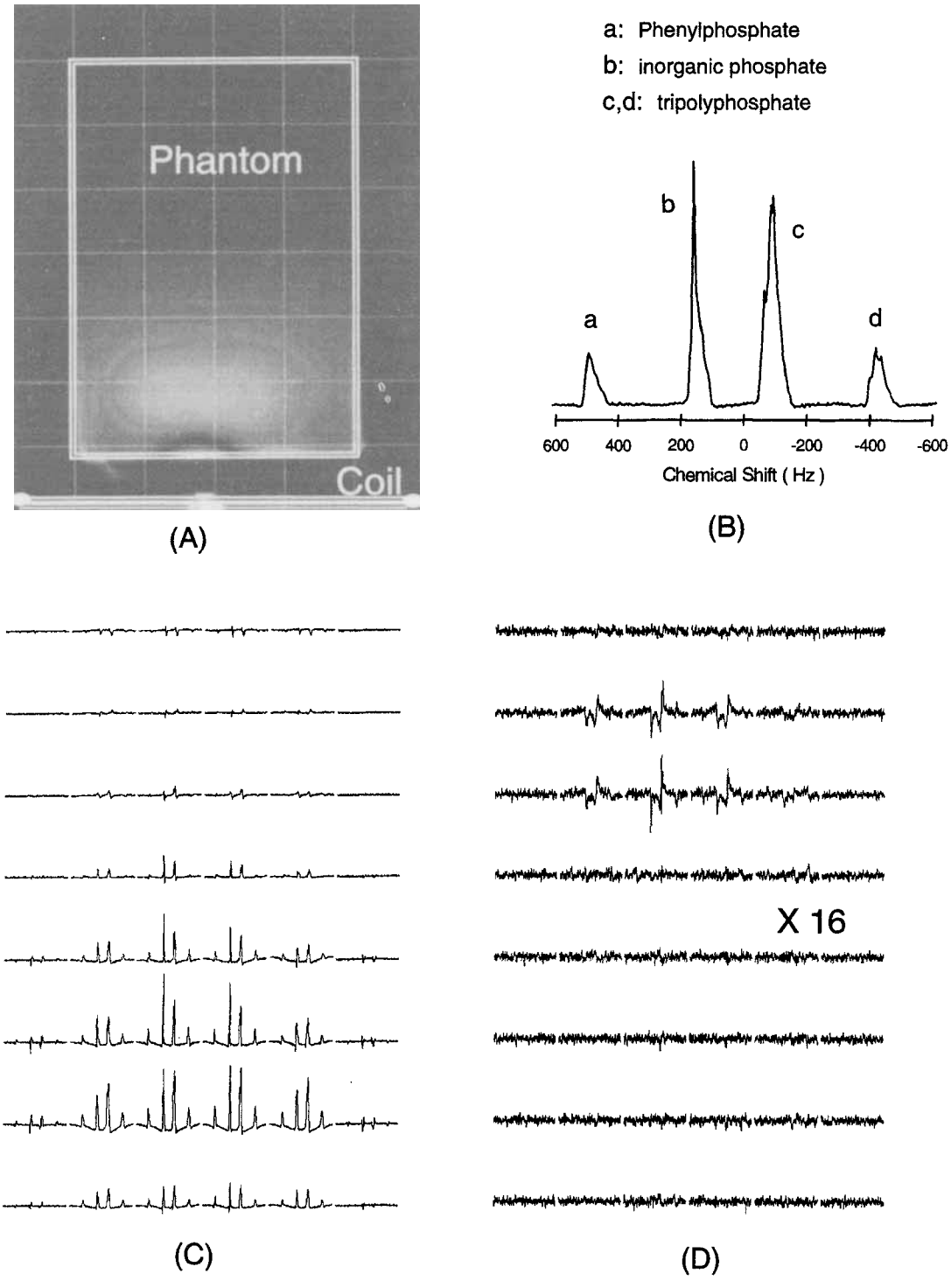

Figure 8. Demonstration of homogeneous excitation by the BIRP pulse using a phantom which contains phenylphosphate, inorganic phosphate and tripolyphosphate in solution. (a) Axial image with the grid overlaid on it to show the positions of the $2.5 \times 2.5 \times 2.5$ cm^3 voxels and the phantom setup. (b) Nonlocalized spectrum using a 45° BIRP pulse. (c and d) Subset of three-dimensional spectra corresponding to the voxels highlighted in (a), with (c) 45° and (d) 180° BIRP pulses. The spectra in (d) are magnified 16 times compared to the spectra in (c).

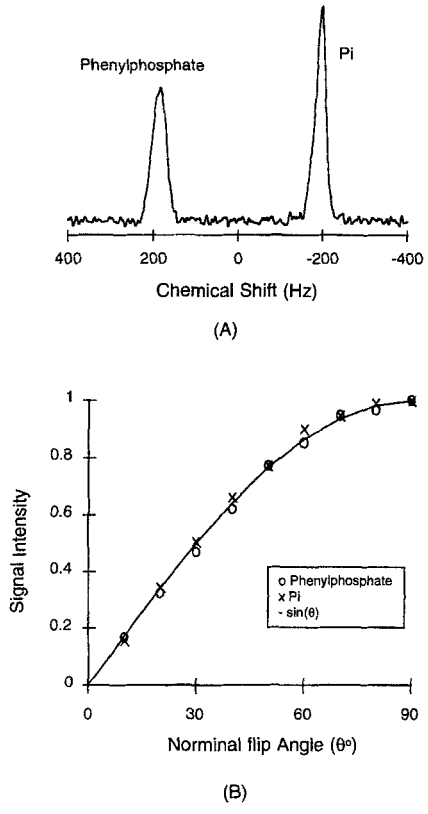

Figure 9. (a) A nonlocalized ^{31}P spectrum from a 5 ml phenylphosphate and inorganic phosphate solution which shows the frequency offset of these two resonances. (b) ^{31}P signal intensity from phenylphosphate and inorganic phosphate as a function of the nominal flip angle, $\theta°$. Signal intensities were normalized to signal intensity obtained with a 90° flip angle.

enhancement factor[56] thus enabling us to validate our technique. The long TR (20 s) of this experiment results in negligible NOE enhancement when the decoupler duration is 250 ms in the absence of the constant component of bilevel decoupling. NOE enhancement caused by low-level irradiation of ^{1}H is shown in the spectra from the same two voxels in Fig. 12(c) and (e). Results from four normal volunteers are summarized in Table 3.

NOE enhancement is associated with relaxation mechanisms related to dipolar coupling, especially dipolar coupling between ^{31}P and solvent (water) ^{1}H nuclei.[57] The degree of NOE enhancement is related to the extent to which dipolar interactions contribute to relaxation relative to other mechanisms like chemical shift anistropy. The maximum η (1.24) occurs in the extreme narrowing limit if the only relaxation mechanism is dipolar coupling. In the extreme narrowing limit, the observed η provides a measure of the relative contributions of dipolar and other mechanisms of relaxation.[58] Moreover, η and T_1 among hepatic metabolites and muscle PCr is shown in Fig. 13. These values are strongly correlated (r=0.90) and indicate that dipolar mechanisms contribute strongly to relaxation in GPEth, GPChol and PCr, moderately to relaxation in PMEs, and little to relaxation in Pi and NTPs.

Quantitation of Hepatic Metabolites

To validate the quantitation procedure, a 2 l spherical phantom containing 100.3 mM inorganic phosphate solution (T_1=6.9 s, measured by the variable nutation angle method) was placed under the coil. The relative position of

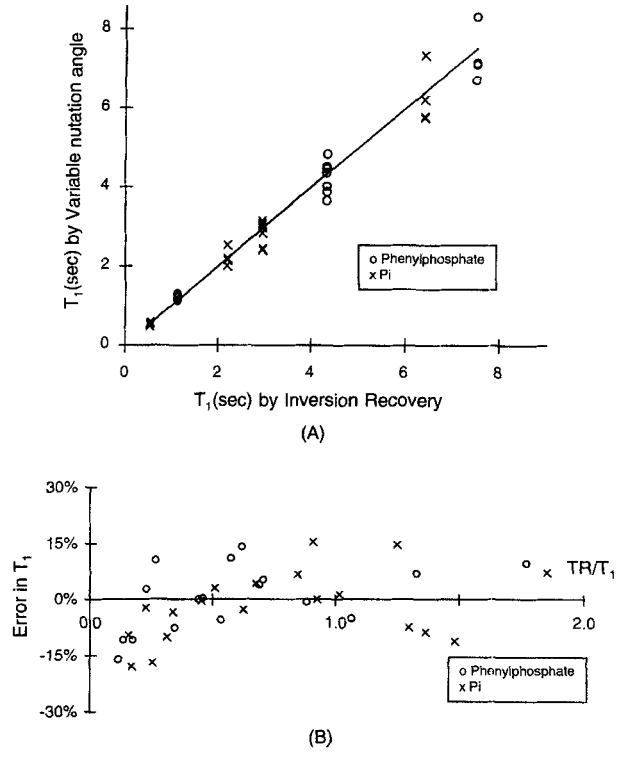

Figure 10. Comparison of T_1 measurements obtained by the variable nutation angle method and by the standard inversion-recovery method. (a). Measurements were made on four 5 ml samples of phenylphosphate and inorganic phosphate doped with different amounts of $NiCl_2$ to give a range of T_1 values from 0.5 to 7.5 s. The diagonal line is the line of identity. The coefficients of variation of T_1 measurements ranged from 5.4% for phenylphosphate at 1.1 s to 11.8% for Pi at 6.4 s. The percentage by which T_1 measurements made by the variable nutation angle method differ from those obtained by inversion-recovery is plotted in (b) as function of TR/T_1.

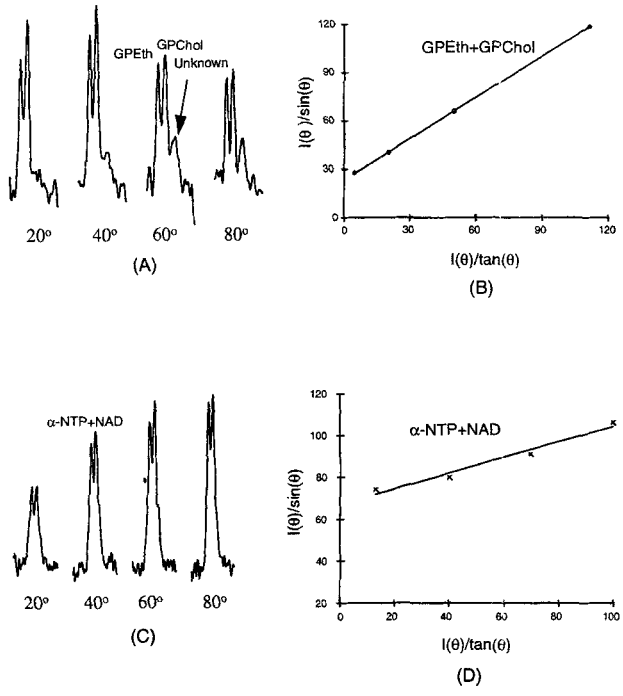

Figure 11. T_1 measurements obtained with four different flip angles in localized ^{31}P spectra from (a) the peak GPEth+GPChol +unknown obtained with TR=1.0 s and (c) α-NTP+NAD obtained with TR=0.5 s. The corresponding plots of $I(\theta/\sin)\theta$ against $I(\theta)/\tan(\theta)$ are shown in (b) and (d).

the coil to the surface of the standard phantom shown in Fig. 14(a) was similar to the relative position of the coil to the surface of the liver *in vivo* (Fig. 2). Three-dimensional CSI datasets from seven different voxel sizes ($2\times2\times2$–$5\times5\times5$ cm^3) were acquired with an $8\times8\times8$ matrix, 512 time points, a sweep width ±1kHz, a TR=1 s, one acquisition for each phase encoding step, and a 45° nutation angle at the depth of 8.0 cm from the coil. One voxel in each three-dimensional CSI experiment, having the same distance to the coil as shown in Fig. 14(a), was used to evaluate the accuracy of the quantitation program. Figure 14(b) shows the results of this experiment. PSF corrections are only needed for voxel sizes of $4\times4\times4$ cm^3 and larger in this phantom setup. To further evaluate the reliability of the quantitation and PSF correction procedures, we repeated this experiment with three different coils (another 15 cm coil and two 12 cm coils) and different relative positions of the phantom to the coils. The results of these three experiments are similar to those of the first which is shown in Fig. 14(b). The average concentration obtained by these four studies on voxel sizes of $4\times4\times4$ cm^3 and larger was 125.7±6.6 mM for no PSF corrections and 103.0±4.3 mM after the PSF corrections. The average PSF correction factor for voxel sizes of $4\times4=4$ cm^3 and larger was 21%.

Taking into account the measured values of T_1 and the measured NOE enhancements, the molar concentrations of hepatic metabolites in proton-decoupled ^{31}P spectra were calculated using eq. (8). The results are summarized in Table 3. Molar concentrations were calculated using the mean values of T_1 and η obtained in separate studies. The CVs of the concentrations shown in Table 3 are therefore measures of inter-individual variations in the fractions of ^{31}P signal in the various metabolites plus variations introduced by reference signal measurements and by corrections for B_1 field and point spread effects. Nevertheless, they are on average only slightly larger than the variations in the long-term individual temporal reproducibility studies shown in column (3) in Table 2. The average PSF correction factor for hepatic metabolites using voxels of 64 cm^3 and larger was 23%. This factor was quite similar to that obtained in the phantom [Fig. 14(b)], which for similar voxel sizes was 21%. Although the phantom experiment can not entirely

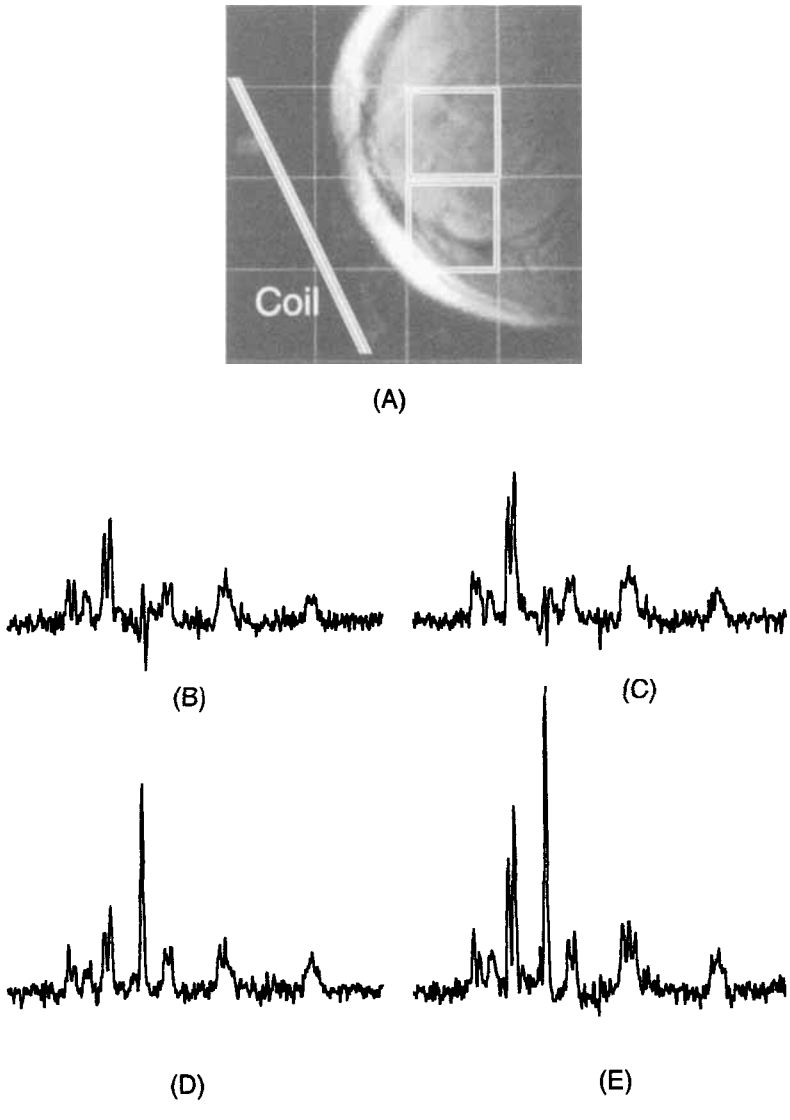

Figure 12. Example of NOE enhancement measurement. (a) Axial image with the grid overload on it to show the position of the 4×4 cm^2 voxels. The coil position is also indicated. The spectra corresponding to the highlighted voxels containing mostly chest wall muscle (bottom) and only liver (top) without continuous ^{1}H irradiation applied are shown in (b) and (d). (c) and (e) are the corresponding spectra with continuous ^{1}H irradiation applied.

Table 3. T_1, NOE enhancement and molar concentration of human hepatic ^{31}P metabolites (mean±SD). Concentrations were calculated using eq. (8) and taking the mean values of T_1 and of NOE enhancement obtained in separate studies. CVs (%) are indicated

Metabolites	T_1 (s) (n=4)	NOE enhancement (n=4)	Concentration (mmol/l of liver) (n=6)
PME_1	2.2±1.1	0.30±0.19	1.2(33%)
PME_2	2.3±0.8	0.47±0.03	1.1(9%)
PME	2.1±0.9	0.34±0.04	2.4(17%)
Pi	0.8±0.2	0.17±0.16	2.8(18%)
GPEth	5.6±1.8	0.59±0.28	2.8(25%)
GPChol	6.6±1.1	0.73±0.28	3.5(17%)
Unknown	2.0±1.0[a]	0.34 (n=2)[a]	1.4(65%)
PDE	6.1±1.3	0.63±0.07	7.6(22%)
PCr[b]	6.3±0.4	0.59±0.11	—
γ-NTP	0.4±0.1	0.21±0.08	3.7(16%)
α-NTP	0.6±0.1	0.36±0.03	3.8(6%)[c]
NAD	2.6±1.4[a]	0.55±0.1[a]	1.1(6%)[c]
β-NTP	0.4±0.1	0.21±0.09	3.8(8%)

[a]Estimated from the peak height.
[b]From chest wall muscle.
[c]Calculated assuming α-NTP is the same as γ-NTP and β-NTP.

reproduce the *in vivo* situation where other tissues outside of the liver may contribute signals to the spectrum, it should be noted that even the strongest signal from the chest wall muscle, that of PCr, is negligible in the localized liver spectrum.

DISCUSSION

These experiments demonstrate that it is possible to obtain ^{1}H-decoupled, NOE-enhanced, phospholipid-saturated, ^{31}P spectra of human liver that are consistently of high quality and are reproducible within relatively small coefficients of variation. The major separate components of the PME and PDE regions are clearly resolved. Molar concentrations of metabolites were obtained by accurately localizing spectra in three dimensions using CSI, correcting for point-spread effects, and directly measuring T_1 and η. A strong correlation between T_1 and η permits estimates of the relative contributions of the dipolar coupling mechanism to ^{31}P relaxation in hepatic metabolites.

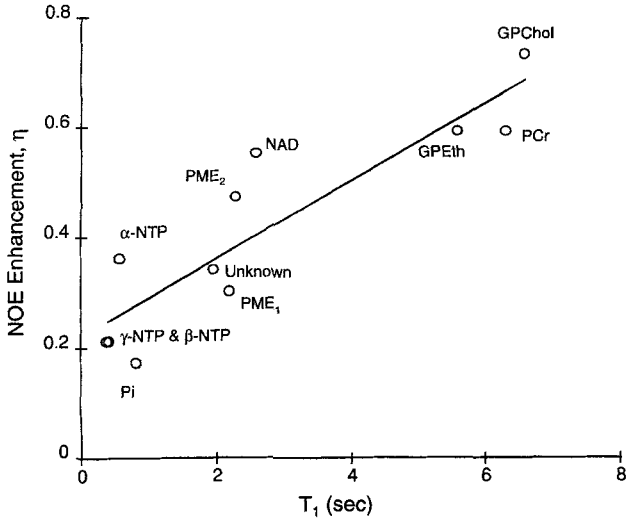

Figure 13. Relation of T_1 and η (mean values from Table 3). The line was estimated with a least squares linear regression method (r=0.90).

A number of reports have indicated the potential value of ^{31}P in clinical studies.[1–24]. The improvements in resolution and S/N obtained with ^{1}H-decoupling and NOE-enhancement make it feasible to obtain information about hepatic metabolites not previously available *in vivo*, and should improve the ability of ^{31}P MRS to characterize hepatic diseases.

The mean human hepatic NTP concentration of 3.7 mmol/l of liver is about 30% higher than previously reported in studies using ISIS[35,36] or one-dimensional CSI[8] for localization, and higher than the 2–2.5 mmol/kg weight reported in studies of tissue extracts.[59] However, hepatic NTP readily decreases under ischemic conditions,[51] so we believe that the *in vivo* concentration is likely to be closer to the value we obtained. The GPEth and GPChol concentrations we obtained (2.8 and 3.5 mmol/l of liver, respectively) are about 20% higher than reported in tissue extract studies.[51]

The T_1 values of ^{31}P we measured in human hepatic NTPs are in good agreement with those previously reported in coupled spectra *in vivo*, which varied from about 0.4 to 0.6 s.[35,36,60–62] However, our values for T_1s of PME, PDE and Pi are quite different from some of those reported in the literature which are themselves quite variable. This is particularly the case for PDE, the reported T_1s of which were 1.4,[35,60] 1.9,[36] 2.0[61] and 8.6.[62] The T_1 of PCr we measured in chest wall muscle (6.3 s) is quite similar to that reported in skeletal muscle.[56] Moreover, the long T_1 we measured in hepatic GPChol (6.6 s) is similar to that reported in skeletal muscle.[56] We believe that the short T_1s of hepatic PDE reported in most previous studies may have been a consequence of inability to resolve GPEth and GPChol from underlying phospholipid signals and/or failure to use acquisition parameters appropriate for the measurement of long T_1. Indeed, a long T_1 of hepatic PDE (8.6 s) was obtained in a subject studied using inversion-recovery[62] and a T_1 of ~7 s was deduced in studies using a wide range of TR values.[63]

The NOE enhancement factor of 0.59 in chest wall muscle PCr is similar to that reported in chest wall[28] and calf[27,56] muscle. Strong enhancement of hepatic GPEth and GPChol signals were observed (~0.6–0.7), moderate enhancement of PME signals (0.3–0.5) and slight enhancement of Pi and NTP signals (~0.2). This pattern, and the degree to which the same metabolite undergoes NOE enhancement, are different from those in calf muscle[27,56] and brain.[29] For example, NTP signals in muscle undergo considerably greater enhancement (~0.5)[56] than in liver. This indicates that the relative contribution of dipolar coupling to ^{31}P relaxation of a particular metabolite may differ in different tissues, and that η must be measured in the tissue of interest in order to obtain a correction factor for calculation of molar concentrations.

The accuracy and errors of the measured concentrations are affected by the accuracy and errors of the spatial volume localization, the signal integration, the T_1 measurement, the NOE measurement and the PSF correction. The accuracy of the volume, which is defined by gradients in three dimensions, has been calibrated on our system and the error is less than 3% in each dimension. The reliability and reproducibility of signal integration were estimated using simulated hepatic ^{31}P spectra which were comparable in resolution and S/N to *in vivo* spectra. The variations are approximately 7% for isolated and 15% for overlapping

peaks. The accuracy of the PSF correction in the phantom studies was high, the mean corrected concentration was within 3% of the actual one. In our reported hepatic metabolite concentrations, we used mean values of T_1 and η determined in separate series of experiments. The coefficients of variation of the T_1 and η measurements averaged about 30%. Since the T_1 and η are correlated, the propagation of these variations into concentration calculations is difficult to determine. To obtain some idea of the extent to which errors in T_1 and η might affect the molar concentration, we calculated concentrations under four conditions: (i) no correction for saturation effect and NOE enhancement; (ii) correction for NOE enhancement only; (iii) correction for saturation effect only; and (iv) correction for both saturation effect and NOE enhancement. The results are shown in Fig. 15. Since the TR of the measurement (1 s) is smaller than $5T_1$ of all the hepatic metabolites, the calculated concentration without correction for the saturation effect will underestimate the result. The calculated concentration without correcting for NOE enhancement will overestimate the result. Correction for both results in concentrations that are different from the uncorrected ones by 25% for PME, 8% for Pi, 50% for PDE and ~15% for NTP. Thus, T_1 and η corrections have opposite effects on molar quantitation. This, combined with the fact that T_1 *and* η are highly correlated (Fig. 13) implies that their variations are not independent and probably do not have additive effect on errors in molar quantitation. A potential practical application of the result in Fig. 15 is that, if one performs NOE enhancement then under these experimental conditions the uncorrected concentration will be within 25 % of the concentration corrected for T_1 and η, except for PDE (which has very long T_1 and high η).

In clinical studies in which molar quantitation is desired, it is not possible to measure T_1 and NOE enhancement in each subject. However, the strong correlation between T_1

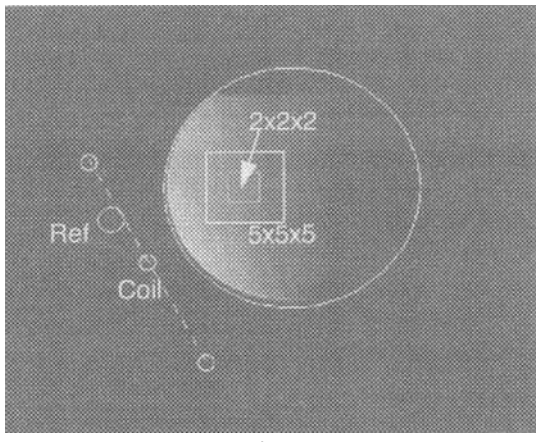

(A)

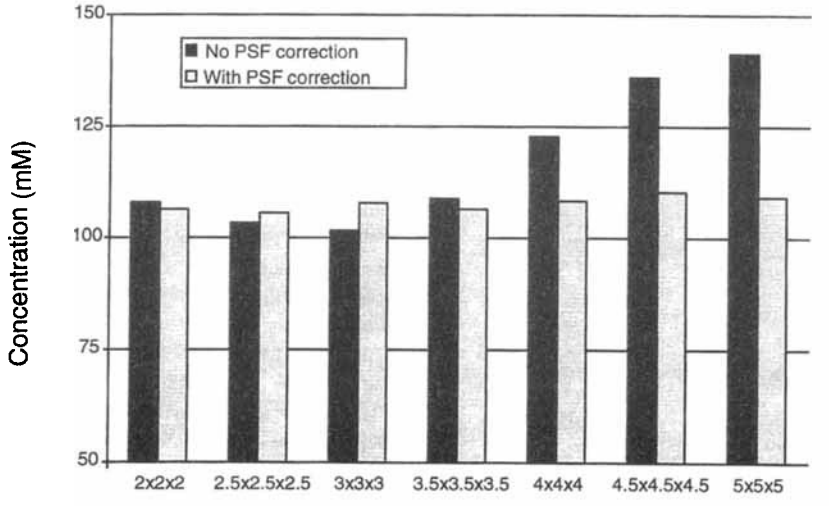

(B)

Figure 14. Example of a phantom experiment to validate the quantitation procedure. (a) An axial image with squares to show the size and location of the selected voxels. The circle indicates the position of the sphere for the PSF correction. (b) Results of the absolute concentration measurement with/without PSF correction. The greater point spread effect occurs when the voxel size is larger than 64 cm^3 on this phantom setup. The real concentration in the phantom is 100.3 mM

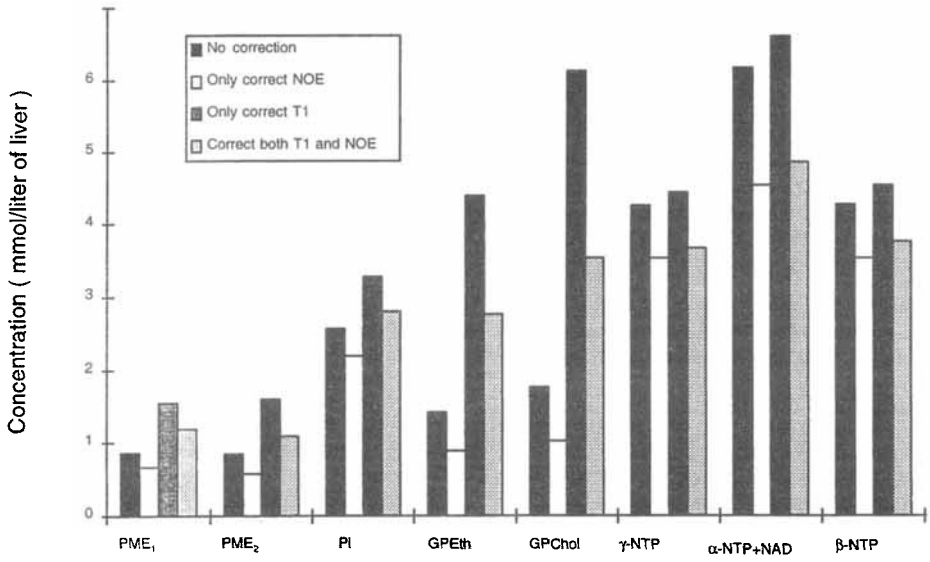

Figure 15. Calculation of molar concentrations (mmol/l of liver) under the conditions: (i) no correction for NOE enhancement and saturation effect; (ii) correction only for NOE enhancement; (iii) correction only for saturation effect; and (iv) correction for both NOE enhancement and saturation effect.

and η suggests that if one of these factors is measured, the other can be derived. Unfortunately, measuring even one of these, at least by standard means (e.g. inversion recovery or progressive saturation in the T_1 measurement and long TR with a saturation pulse sequence in the NOE enhancement measurement) is time consuming. Less time is required if one uses a nonlocalized technique to measure T_1 or NOE enhancement, but this could be a problem because of the different T_1 and NOE enhancements of Pi, GPChol and NTPs in liver and chest wall muscle. The use of a nonlocalized technique is only feasible if one is interested only in the PME region.

An alternative way to obtain NOE enhancement is by using a short TR with a single 180° pulse in the proton channel.[64] The power deposition problem and the difficulty achieving full NOE enhancement are the main concerns with this technique. On the other hand, the variable-nutation angle method is a more rapid way to measure the T_1 than the standard inversion recovery method, but the time is still not fast enough to add the T_1 measurement experiment to each clinical ^{31}P MRS study. To reduce the time requirement, the use of only two nutation angles (at 15 and 60° for T_1/TR=0.1–1.0) has been suggested.[61] Indeed, we found that by selecting the 20 and 60° data from our variable-nutation angle measurement, the T_1s are quite similar to those obtained with four nutation angles (1.5 s vs 2.1 s on PME, 0.8 vs 0.8 s on Pi, 5.8 vs 6.1 s on PDE and 0.4 vs 0.4 s on b-NTP). Considering the time constraints, acceptable S/N within a short period of time and the requirement of localization, the combination of the dual-angle method with two-dimensional CSI localization (8×8 matrix, six acquisition and TR=1 s, the third dimension defined by the sensitive volume of the coil) may permit measurement of T_1 in each ^{31}P MRS study within 15 min. A drawback in liver studies is that the T_1s vary over a wide angle, and it is not possible to optimize TR to obtain both short and long T_1s in one study.

In conclusion, these experiments demonstrate that high quality ^{31}P spectra with good resolution of PME and PDE metabolites can be obtained routinely from human liver using proton-decoupled, NOE-enhanced, phospholipid-saturated ^{31}P acquisitions localized with three-dimensional CSI. A complete approach to absolute quantitation is demonstrated, including measurements of T_1 and η and corrections for point spread effects. The additional information obtained using proton-decoupling and NOE-enhancement should help expand the scope of ^{31}P MRS for the study of hepatic disorders.

Acknowledgements

We thank Ronald McNamara, PhD for assistance in phospholipid saturation pulse and BIRP pulse implementation, Peter Z. Liu and Tariq Javaid, M.S. for assistance in automatic shimming, Chris Elsasser for assistance in coil construction and Michael Garwood, PhD for providing the BIR-4 pulse program. This work was supported in part by NIH grants CA58632, CA54339 and CA41078.

REFERENCES

1. Oberhaensli, R. S., Rajagopalan, B., Taylor, D. J., Radda, G. K., Collins, J. E., Leonard, J. V., Schwarz, H. and Herschkowitz, N. Study of hereditary fructose intolerance by use of ^{31}P magnetic resonance spectroscopy. *Lancet* **1**, 931–934 (1987).
2. Cox, I. J., Bryant, D. J., George, P., Harman, R. R., Hall, A. S., Hodgson, H. J. F., Khenia, S., McArthur, P. and Spencer, D. H. Four-dimensional chemical shift MR imaging of phosphorus metabolites of normal and diseased human liver. *J. Comput. Assist. Tomog.* **12**, 369–376 (1988).
3. Meyerhoff, D. J., Boska, M. D., Thomas, A. M. and Weiner, M. W. Alcoholic liver disease: quantitative image-guided P-31 MR spectroscopy. *Radiology* **173**, 393–400 (1989).
4. Oberhaensli, R., Rajagopalan, B., Galloway, G. J., Taylor, D. J. and Radda, G. K. Study of human liver disease with P-31 magnetic resonance spectroscopy. *Gut* **31**, 463–467 (1990).
5. Angus, P. W., Dixon, R. M., Rajagopalan, B. and Radda, G. K. A study of patients with alcoholic liver disease by P-31

nuclear magnetic resonance spectroscopy. *Clin. Sci.* **78**, 33 (1990).
6. Sakuma, H., Itabashi, K., Takeda, K., Hirano, T., Kinosada, Y., Nakagawa, T., Yamada, M. and Nakano, T. Serial P-31 MR spectroscopy after frucstose infusion in patients with chronic hepatitis. *J. Magn. Reson. Imag.* **1**, 701–704 (1991).
7. Cox, I. J., Menon, D. K., Sargentoni, J., Bryant, D. J., Collins, A. G., Coutts, G. A., Iles, R. A., Bell, J. D., Benjamin, I. S., Gilbey, S., Hodgson, H. J. F. and Morgan, M. Y. Phosphorus-31 magnetic resonance spectroscopy of the human liver using chemical shift imaging techniques. *J. Hepat.* **14**, 265–275 (1992).
8. Rajanayagam, V., Lee, R. R., Ackerman, Z., Bradley, W. G. and Ross, B. D. Quantitative P-31 MR spectroscopy of the liver in alcoholic cirrhosis. *J. Magn. Reson. Imag.* **2**, 183–190 (1992).
9. Brinkmann, G. and Melchert, U. H. A study of T_1-weighted ^{31}P MR spectroscopy from patients with focal and diffuse liver disease. *Magn. Reson. Imag.* **10**, 949–956 (1992).
10. Dufour, J. F., Stoupis, C., Lazeyras, F., Vock, P., Terrier, F. and Reichen, J. Alterations in hepatic fructose metabolism in cirrhotic patients demonstrated by dynamic ^{31}P spectroscopy. *Hepatology* **15**, 835–842 (1992).
11. Kalderon, B., Dixon, B., Rajagopalan, B., Angus, P. W., *Oberhaensli, R. D., Collins, J. E., Leonard, J. V. and Radda,* G. K. A study of galactose intolerance in human and rat liver *in vivo* by ^{31}P magnetic resonance spectroscopy. *Pediat. Res.* **32**, 39–44 (1992).
12. Dixon, R. M., Angus, P. W., Rajagopalan, B. and Radda, G. K. ^{31}P magnetic resonance spectroscopy detects a functional abnormality in liver metabolism after acetaminophen poisoning. *Hepatology* **16**, 943–948 (1992).
13. Munakata, T., Griffiths, R. D., Martin, P. A., Jenkins, S. A., Shields, R. and Edwards, R. H. T. An *in vivo* ^{31}P MRS study of patients with liver cirrhosis: progress towards a non-invasive assessment of disease severity. *NMR Biomed.* **6**, 168–172 (1993).
14. Yamane, Y., Umeda, M., O'uchi, T., Mitsuhima, T., Nakata, K. and Nagataki, S. Phosphorus-31 nuclear magnetic resonance *in vivo* spectroscopy of human liver during hepatitis A virus infection. *Digest. Dis. Sci.* **39**, 33–38 (1994).
15. Boesiger, P., Buchli, R., Meier, D., Steinmann, B. and Gitzelmann, R. Change of liver metabolism after intravenous fructose by ^{31}P magnetic resonance spectroscopy. *Pediat. Res.* **36**, 436–440 (1994).
16. Menon, D. K., Sargentoni, J., Taylor-Robinson, S. D., Bell, J. D., Cox, J., Bryant, D. J., Coutts, G. A., Rolles, K., Burroughs, A. K. and Morgan, M. Y. Effect of functional grade and etiology on *in vivo* hepatic phosphorus-31 magnetic resonance spectroscopy in cirrhosis: biochemical basis of spectral appearances. *Hepatology* **21**, 417–427 (1995).
17. van Wassenaer-van Hall, H. N., van der Grond, J., van Hattum, J., Kooijman, C., Hoogenraad, T. U. and Mali, W. P. ^{31}P magnetic resonance spectroscopy of the liver: correlation with standardized serum, clinical and histological changes in diffuse liver disease. *Hepatology* **21**, 443–449 (1995).
18. Maris, J. M., Evans, A. E., McLaughlin, A. C., D'Angio, G. J., Bolinger, L., Manos, H. and Chance, B. ^{31}P Nuclear magnetic resonance spectroscopy investigation of human neuroblastoma *in situ*. *New Engl. J. Med.* **6**, 1500–1505 (1985).
19. Glazer, G. M., Smith, S. R., Chenevert, T. L., Martin, P. A., Stevens, A. N. and Edwards, R. H. T. Image localized P-31 magnetic resonance spectroscopy of the human liver. *NMR Biomed.* **1**, 184–189 (1989).
20. Dixon, R. M., Angus, P. W., Rajagopalan, B. and Radda, G. K. Abnormal phosphomonoester signals in ^{31}P MR spectra from patients with hepatic lymphoma. A possible marker of liver infiltration and response to chemotherapy. *Brit. J. Cancer* **63**, 953–958 (1991).
21. Francis, I. R., Chenevert, T. L., Gubin, B., Collomb, L., Ensminger, W., Walker-Andrews, S. and Glazer, G. M. Malignant hepatic tumors: P-31 MR spectroscopy with one-dimensional chemical shift imaging. *Radiology* **180**, 341–344 (1991).
22. Cox, I. J., Bell, J. D., Peden, C. J., Iles, R. A., Foster, C. S., Watanapa, P. and Williamson, R. C. N. *In vivo* and *in vitro* ^{31}P magnetic resonance spectroscopy of focal hepatic malignancies. *NMR Biomed.* **5**, 114–120 (1992).
23. Meyerhoff, D. J., Karczmar, G. S., Valone, F., Venook, A., Matson, G. B. and Weiner, M. W. Hepatic cancers and their response to chemoembolization therapy. *Invest. Radiol.* **27**, 456–464 (1992).
24. Schilling, A., Gewiese, B., Berger, G. and Wolf, K. J. Liver tumors: follow-up with P-31 MR spectroscopy after local chemotherapy and chemoembolization. *Radiology* **182**, 887–890 (1992).
25. Luyten, P. R., Bruntink, G., Sloff, F. M., Vermeulen, J. W. A. H., van der Heijden, J. I., den Hollander, J. A. and Heerschap, A. Broadband proton decoupling in human ^{31}P NMR spectroscopy. *NMR Biomed.* **1**, 177–183 (1989).
26. Wicklow, K., Sauter, R., Schneider, M. and Kolem, H. ^{1}H-^{31}P double resonance MRS on the human liver: comparison of different ^{1}H decoupling schemes. *Proc. Soc. Magn. Reson.* **3**, 3312 (1992).
27. Bachert-Baumann, P., Ermark, F., Zabel, H. J., Sauter, R., Semmler, W. and Lorenz, W. J. *In vivo* nuclear Overhauser effect in ^{31}P-{^{1}H} double-resonance experiments in a 1.5 T whole-body MR system. *Magn. Reson. Med.* **15**, 165–172 (1990).
28. Bottomley, P. A. and Hardy, C. J. Proton Overhauser enhancements in human cardiac phosphorus NMR spectroscopy at 1.5 T. *Magn. Reson. Med.* **24**, 384–390 (1992).
29. Murphy-Boesch, J., Stoyanava, R., Srinivasan, R., Willard, T., Vigneron, D., Nelson, S., Taylor, J. S. and Brown, T. R. Proton-decoupled ^{31}P chemical shift imaging of the human brain in normal volunteers. *NMR Biomed.* **6**, 173–180 (1993).
30. Negendank, W. G., Padavic-Shaller, K. A., Li, C. W., Murphy-Boesch, J., Stoyanova, R., Krigel, R. L., Schilder, R. J., Smith, M. R. and Brown, T. R. Metabolic characterization of human non-Hodgkin's lymphomas *in vivo* using proton-decoupled phosphorus magnetic resonance spectroscopy. *Cancer Res.* **55**, 3286–3294 (1995).
31. Bates, T. E., Williams, S. R. and Gadian, D. G. Phosphodiesters in the liver: the effect of field strength on the ^{31}P signal. *Magn. Reson. Med.* **12**, 145–150 (1989).
32. Murphy, E. J., Bates, T. E., Williams, S. R., Watson, T., Brindle, K. M., Rajagopalan, B. and Radda, G. K. Endoplasmic reticulum: the major contributor to the PDE peak in hepatic ^{31}P-NMR spectra at low magnetic field strengths. *Biochim. Biophys. Acta.* **1111**, 51–58 (1992).
33. Murphy, E. J., Rajagopalan, B., Brindle, K. M. and Radda, G. K. Phospholipid bilayer contribution to ^{31}P NMR spectra *in vivo*. *Magn. Reson. Med.* **12**, 282–289 (1989).
34. McNamara, R., Arias-Mendoza, F. and Brown, T. R. Investigation of broad resonances in ^{31}P NMR spectra of the human brain *in vivo*. *NMR Biomed.* **7**, 237–242 (1994).
35. Meyerhoff, D. J., Karczmar, G. S., Matson, G. B., Boska, M. D. and Weiner, M. W. Non-invasive quantitation of human liver metabolites using image-guided ^{31}P magnetic resonance spectroscopy. *NMR Biomed.* **3**, 17–22 (1990).
36. Buchli, R., Meier, D., Martin, E. and Boseiger, P. Assessment of absolute metabolite concentrations in human tissue by ^{31}P MRS *in vivo*. Part II: muscle, kidney. *Magn. Reson. Med.* **32**, 453–458 (1994).
37. Bottomley, P. A., Hardy, C. J., Roener, P. B. and Weiss, R. G. Problems and experiences in human ^{31}P spectroscopy. *NMR Biomed.* **2**, 284–289 (1989).
38. Brown, T. R. Practical applications of chemical shift imaging. *NMR Biomed.* **5**, 238–243 (1992).
39. Brown, T. R., Kincaid, B. M. and Ugurbil, K. NMR chemical shift imaging in three dimensions. *Proc. Natl. Acad. Sci. USA* **79**, 3523–3526 (1982).
40. Schilling, V. A., Gewiese, B., Stiller, D., Romer, T. and Wolf, K. J. Influence of nutritional status on the ^{31}P-MR spectrum of the healthy liver. *Fortschr. Rontgenstr.* **153**, 369–372 (1990).
41. Liu, Z., Javaid, T., Hu, J. and Brown, T. R. CSI-autoshim procedure for body and surface coil. *Proc. Soc. Magn. Reson.* **3**, 1174 (1994).
42. Hu, J., Javaid, T., Arias-Mendoza, F., Liu, Z., McNamara, R. and Brown, T. R. A fast, reliable automatic shimming procedure using ^{1}H chemical shift imaging. *J. Magn. Reson. B.* **108**, 213–219 (1995).
43. Staewen, R. S., Johnson, A. J., Ross, B. D., Parrish, T., Merkle, H. and Garwood, M. Three-dimensional FLASH imaging using a single surface coil and a new adiabatic pulse, BIR-4. *Invest. Radiol.* **25**, 559–567 (1990).
44. Bottomley, P. A. and Ouwerkerk, R. BIRP, an improved

implementation of low-angle adiabatic (BIR-4) excitation pulses. *J. Magn. Reson.* **103**, 242–244 (1993).
45. Christensen, K. A., Grant, D. M., Schulman, E. M. and Walling, C. Optimal determination of relaxation times of Fourier transform nuclear magnetic resonance. Determination of spin-lattice relaxation times in chemically polarized species. *J. Phys. Chem.* **78**, 1971–1978 (1974).
46. Gupta, R. K. A new look at the method of variable nutation angle for the measurement of spin-lattice relaxation times using Fourier transform NMR. *J. Magn. Reson.* **25**, 231–235 (1977).
47. Vigneron, D. B., Nelson, S. J., Murphy-Boesch, J., Kelley, D. A. C., Kessler, H. B., Brown, T. R. and Taylor, J. S. Chemical shift imaging of human brain: axial, sagittal, and coronal P-31 metabolite image. *Radiology* **177**, 643–649 (1990).
48. Moon, R. B. and Richards, J. H. Determination of intracellular pH of ^{31}P magnetic resonance. *J. Biol. Chem.* **248**, 7276–7278 (1973).
49. Murphy-Boesch, J., Jiang, H., Stoyanova, R. and Brown, T. R. Quantitation of phosphorus metabolites from CSI spectra with corrections for point spread effects and B_1 inhomogeneity. *Magn. Reson. Med.* (1995) (submitted).
50. Ramo, S., Whinnery, J. R. and Van Duzer, T. Fields and waves in communication electronics. Wiley, New York (1965).
51. Bell, J. D., Cox, I. J., Sargentoni, J., Peden, C. J., Menon, D. K., Foster, C. S., Watanapa, P., Iles, R. A. and Urenjak, J. A. ^{31}P and ^{1}H-NMR investigation *in vitro* of normal and abnormal human liver. *Biochim. Biophys. Acta.* **1225**, 71–77 (1993).
52. Petersen, A., Kappler, F., Szwergold, B. S. and Brown, T. R. Fructose metabolism in the human erythrocyte. *Biochem. J.* **284**, 363–366 (1992).
53. Lautt, W. W. Hepatic vasculature: a conceptual review. *Gastroenterology* **73**, 1163–1169 (1977).
54. Cohen, S. M. Application of nuclear magnetic resonance to the study of liver physiology and disease. *Hepatology* **3**, 738–749 (1983).
55. Dagnelie, P. C., Menon, D. K., Cox, I. J., Bell, J. D., Sargentoni, J., Coutts, G. A., Urenjak, J. and Iles, R. A. Effect of L-alanine infusion on ^{31}P magnetic resonance spectra of *normal human liver: toward biochemical pathology in vivo. Clin. Sci.* **83**, 183–190 (1992).
56. Brown, T. R., Stoyanova, R., Greenberg, T., Srinvasen, R. and Murphy-Boesch, J. NOE enhancements and T_1 relaxation times of phosphorylated metabolites in human calf muscle at 1.5 Tesla. *Magn. Reson. Med.* **33**, 417–421 (1995).
57. Hart, P. A. Phosphorus relaxation methods: conformation and dynamics of nucleic acids and proteins. In *Phosphorus-31 NMR*, ed. by D. G. Gorenstein, pp. 317–347. Academic Press, San Diego, CA.
58. Mathur-De Vre, R., Maerschalk, C. and Delporte, C. Spin-lattice relaxation times and nuclear Overhauser enhancement effect for ^{31}P metabolites in model solutions at two frequencies: implications for *in vivo* spectroscopy. *Magn. Reson. Imag.* **8**, 691–698 (1990).
59. Hultman, E., Nilsson, L. H. and Sahlin, K. Adenine nucleotide content of human liver. Normal values and fructose-induced depletion. *Scand. J. Clin. Lab. Invest.* **35**, 245–251 (1975).
60. Buchthal, S. D., Thoma, W. J., Taylor, J. S., Nelson, S. J. and Brown, T. R. *In vivo* T_1 values of phosphorus metabolites in human liver and muscle determined at 1.5 T by chemical shift imaging. *NMR Biomed.* **2**, 298–304 (1989).
61. Bottomley, P. A. and Ouwerkerk, R. The dual-angle method for fast, sensitive T_1 measurement *in vivo* with low-angle adiabatic pulses. *J. Magn. Reson. B* **104**, 159–167 (1994).
62. van Ormondt, D., de Beer, R., Marien, A. J. H., den Hollander, J. A., Luyten, P. R. and Vermeulen, J. W. A. H. Two-dimensional approach to quantitation of inversion-recovery data. *J. Magn. Reson.* **88**, 652–659 (1990).
63. Cox, I. J., Coutts, G. A., Gadian, D. G., Ghosh, P., Sargentoni, J. and Young, I. R. Saturation effects in phosphorus-31 magnetic resonance spectra of the human liver. *Magn. Reson. Med.* **17**, 53–61 (1991).
64. Kolem, H., Schneider, M., Wicklow, K. and Sauter, R. *Fast in vivo* phosphorus spectroscopy using nuclear Overhauser enhancement. *Proc. Soc. Magn. Reson.* **2**, 889 (1990).